Journal of Theoretical Biology 473 (2019) 67–79

Contents lists available at ScienceDirect

Journal of Theoretical Biology

journal homepage: www.elsevier.com/locate/jtb

Computational model of the dual action of PTH — Application to a rat model of osteoporosis

Silvia Trichilo[a], Stefan Scheiner[b], Mark Forwood[c], David M.L. Cooper[d], Peter Pivonka[a,e,*]

[a] St Vincent's Department of Surgery, The University of Melbourne, Clinical Science Building, 29 Regent Street, Fitzroy VIC 3065, Australia
[b] Institute for Mechanics of Materials and Structures, Vienna University of Technology (TU Wien), Karlsplatz 13/202, 1040 Vienna, Austria
[c] School of Medical Science, Griffith University, Gold Coast Campus, Parklands Drive, Southport QLD 4222, Australia
[d] Department of Anatomy Physiology and Pharmacology, University of Saskatchewan, 107 Wiggins Road, Saskatoon SK S7N 5E5, Canada
[e] School of Chemistry, Physics and Mechanical Engineering, Queensland University of Technology, 2 George Street, Brisbane QLD 4000, Australia

ARTICLE INFO

Article history:
Received 17 September 2018
Revised 18 April 2019
Accepted 19 April 2019
Available online 19 April 2019

Keywords:
Bone modelling
Bone remodelling
Intermittent administration of PTH
Rat model
Predictive simulation

ABSTRACT

This paper presents a pharmacokinetic/pharmacodynamic (PK/PD) model of the action of PTH(1-34) on bone modelling and remodelling, developed for quantitatively investigating the dose- and administration pattern-dependency of the bone tissue response to this drug. Firstly, a PK model of PTH(1-34) was developed, accounting for administration via subcutaneous injections. Subsequently, the PK model was coupled to a (mechanistic) bone cell population model of bone modelling and remodelling, taking into account the effects of PTH(1-34) on the differentiation of lining cells into active osteoblasts, on the apoptosis of active osteoblasts, and on proliferation of osteoblast precursors, as well as on the key regulatory pathways of bone cell activities. Numerical simulations show that the coupled PK/PD model is able to distinguish between continuous and intermittent administration patterns of PTH(1-34), in terms of yielding both catabolic bone responses (if drug administration is carried out continuously) and anabolic bone responses (if drug administration is carried out intermittently). The model also features a non-linear relation between bone gain and drug dose (as known from experiments); doubling the dose from 80 μg/kg/day to 160 μg/kg/day induced a 1.3-fold increase of the bone volume-to-total volume ratio. Furthermore, the model presented in this paper confirmed that bone modelling represents an essential mechanism of the anabolic response of bone to PTH(1–34) administration in rat models, and that the large amount of bone formation observed in such models cannot be explained via remodelling alone.

1. Introduction

The hormone secreted by the parathyroid glands, usually referred to as parathyroid hormone, or, in short, PTH, is known to be essential for calcium homeostasis. In particular, it is able to stimulate increased osteoclast activity, which, in turn, leads to the release of calcium ions stored in the bone matrix (Mundy and Guise, 1999). On the other hand, PTH has also been identified as a key substance in pharmacological applications. PTH peptides, namely PTH(1-34), also known as teriparatide, and PTH(1-84), were the first anabolic agents approved by drug administration agencies for the treatment of degenerative bone diseases (such as osteoporosis), see, e.g., (U.S. Food and Drug Administration, 2019; European Medicines Agency, 2019). However, depending on the applied administration pattern (i.e., on the periodicity of its exposure onto the body), PTH may induce fundamentally opposed bone responses (Silva and Bilezikian, 2015).

Continuous infusion of PTH and conditions such as hyperparathyroidism lead to catabolic responses, hence to increased bone resorption (Potts, 2005). In more detail, it is known from both *in vitro* and *in vivo* studies that PTH does not directly activate osteoclasts, but it enhances bone resorption indirectly, via the RANK-RANKL-OPG pathway (McSheehy and Chambers, 1986; Xiong and O'Brien, 2012; Hofbauer and Schoppet, 2004). In this context, it should be mentioned that receptors of PTH were found on osteoblast precursor cells, active osteoblasts, lining cells and osteocytes (Bringhurst et al., 2016). Continuous infusion of PTH actually leads to modulation of the RANK-RANKL-OPG pathway towards an increased RANKL/OPG ratio, thereby promoting osteoclastogenesis and inducing, in further consequence, increased bone resorption (Lee and Lorenzo, 1999; Huang et al., 2004).

In contrast, daily subcutaneous injections of PTH are known to lead to anabolic responses in bone tissue, hence to increased bone formation (Dempster et al., 1993; Jilka, 2007). Similar to

* Corresponding author at: School of Chemistry, Physics and Mechanical Engineering, Queensland University of Technology, 2 George Street, Brisbane QLD 4000, Australia.

https://doi.org/10.1016/j.jtbi.2019.04.020
0022-5193/

continuous PTH exposure, intermittent administration of PTH causes an increased bone turnover. However, in the latter case, PTH acts directly on osteoblasts to promote osteoblastogenesis. Namely, the anti-apoptotic action of PTH involves the phosphorylation and deactivation of the pro-apoptotic protein Bad, increased expression of survival genes like B-cell lymphoma 2 (Bcl-2), increased expression of Runt-related transcriptor factor 2 (Runx2), downregulation of the apoptosis inducer cell cycle and apoptosis regulatory protein (CARP-1) and increased DNA repair (Bellido et al., 2003; Jilka, 2007; Schnoke et al., 2009; Sharma et al., 2013). Furthermore, studies performed on rats treated with intermittent PTH showed an increased number of osteoblasts on bone surfaces associated with a decreased fraction of lining cells, without indication of increased osteoblast proliferation (Leaffer et al., 1995; Dobnig and Turner, 1995; Kim et al., 2012). In addition, recent studies have identified effects of PTH on the canonical Wnt/β-catenin signalling pathway via sclerostin, a secreted glycoprotein primarily produced by osteocytes and acting as bone formation inhibitor (Poole et al., 2005; Costa and Bilezikian, 2012). Sclerostin inhibits bone formation by antagonising the Wnt/β-catenin anabolic signalling pathway, which modulates osteoblast proliferation, differentiation and survival (Kramer et al., 2010; Glass et al., 2005). PTH is believed to reduce sclerostin concentration and consequently reduce its inhibiting effect on bone formation (Canalis et al., 2007; Ogura et al., 2016). In the absence of Wnt signalling, β-catenin is phosphorylated by the protein complex formed by Axin, adenomatous polyposis coli (APC) and glycogen synthase kinase 3 (GSK-3). If, however, Wnt signalling is present, the cytoplasmic protein disheveled (Dvl) is activated, disrupting the Axin-APC-GSK-3 complex from phosphorylating β-catenin. As a result, β-catenin translocates to the nucleus, regulating the transcription of Wnt target genes (Costa and Bilezikian, 2012; Cadigan and Liu, 2006).

While the dual action of PTH is well-known (as documented by the above-mentioned studies), the exact underlying molecular and intercellular mechanisms are still unclear, at least in quantitative terms. Thus, no comprehensive picture of the mechanisms responsible for this clinical paradox has been drawn yet (Qin et al., 2004; Poole and Reeve, 2005). Attempting to remedy this unsatisfactory situation, a number of mathematical models were proposed, in order to better understand and even quantitatively predict the effects of PTH administration on bone cells, see, e.g., (Rattanakul et al., 2003; Komarova, 2005; Potter et al., 2005) and similar works. Despite the progress achieved in the past 15 or so years, most of those models neither consider the involved biochemical pathways in appropriate detail, nor were they validated through comparison of model predictions to experimental data. In this paper, we attempt to fill both gaps.

In particular, a new mathematical model is presented which allows for shedding light on the intercellular and tissue-scale mechanisms contributing to the dual action of PTH, and its effects on the bone tissue development in rat models of osteoporosis. Thereby, the focus is on teriparatide, or recombinant human PTH(1-34), which is the first anabolic drug in a new class of agents inducing bone formation (Eli Lilly, 2014). PTH(1-34) is administered to patients suffering from severe osteoporosis, particularly to women with postmenopausal osteoporosis (PMO), who are believed to be at high risk of fracture. In clinical practice, it is administered daily, based on single subcutaneous injections (at a dose of 20 μg/day). In terms of the modelling strategy, two concepts are combined. On the one hand, focussing on PTH(1-34), a one-compartment PK model was considered, allowing for (predictively) estimating the availability of PTH(1-34) in the blood serum if administration occurs in the form of intermittent injections, described in Section 2.1. Then, the effect of administering PTH(1-34) on the overall PTH serum concentration is described, in Section 2.2, after which a so-called bone cell population model (BCPM), adapted from previous works (Pivonka et al., 2008; 2010), is introduced. In more detail, those works were extended in order to account for both bone modelling and remodelling responses, and to take into account the differentiated effects of PTH(1-34) on those two processes, see Section 2.3. Emulating osteoporosis in rat models is standardly done through ovariectomy, and Section 2.4 describes how ovariectomy is considered in our model. Our new model, hereafter optionally referred to as mechanistic pharmacokinetic/pharmacodynamic (PK/PD) model (Danhof et al., 2007), is calibrated and validated based on experimental data on intermittent and continuous administration of PTH(1-34) in healthy and ovariectomized (OVX) rats, involving different doses and different starting points of drug administration; the considered data is presented in Section 2.5. Numerical studies are presented in Section 3, and all results are discussed in reasonable detail in Section 4. Conclusions and a brief outlook to possible future research directions end the paper, see Section 5.

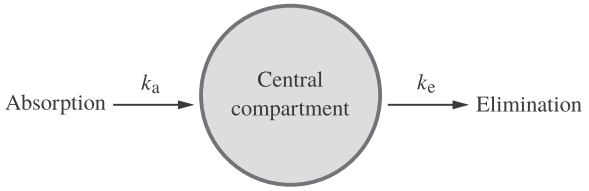

Fig. 1. Schematic representation of the one-compartment PK model of PTH(1-34), showing the absorption and elimination processes the drug is subjected to.

2. Methods

2.1. Pharmacokinetics model for intermittent administration of PTH(1-34)

Following the results of previous works showing no significant difference between the use of a one-compartment and a two-compartment PK model for PTH(1-34) (Satterwhite et al., 2010; Stratford et al., 2014), a one-compartment representation is considered in this paper, see Fig. 1. This one compartment, also referred to as central compartment, represents the blood and all highly perfused tissues that rapidly equilibrate with the drug. Since intermittent administration of PTH(1-34) standardly occurs via subcutaneous injections, the PK model accounts for both drug absorption (from the subcutaneous site into the blood stream) and drug elimination processes. Absorption and elimination are both assumed to be first-order reactions. Mathematically, the above-elaborated considerations lead to a PK model consisting of one ODE describing the absorption of PTH(1-34) from the subcutaneous tissue into the blood serum,

$$\frac{\mathrm{d}m_{\mathrm{PTH,sub}}}{\mathrm{d}t} = -k_{\mathrm{a}}\, m_{\mathrm{PTH,sub}}\, F, \tag{1}$$

and one ODE describing the change of the PTH(1-34) concentration in the serum,

$$\frac{\mathrm{d}C_{\mathrm{PTH,ser}}}{\mathrm{d}t} = \frac{k_{\mathrm{a}}\, m_{\mathrm{PTH,sub}}\, F}{M_{\mathrm{PTH}}\, V_{\mathrm{d}}} - k_{\mathrm{e}}\, C_{\mathrm{PTH,ser}}\,. \tag{2}$$

In Eqs. (1) and (2), $m_{\mathrm{PTH,sub}}$ is the mass of PTH in the subcutaneous tissue, $C_{\mathrm{PTH,ser}}$ is the molar concentration of PTH in the serum, M_{PTH} is the molecular weight of PTH(1-34), $M_{\mathrm{PTH}} = 4117.8$ g/mol (Eli Lilly, 2014), F is the bioavailability, and V_{d} represents the volume of distribution within the compartment; hence, V_{d} relates the amount of drug in the body to the drug concentration measured in the biological fluid (Trichilo and Pivonka, 2018). Furthermore, variables k_{a} and k_{e} are the absorption and the elimination rate constants. In pharmacology, a frequently used measure to quantify the

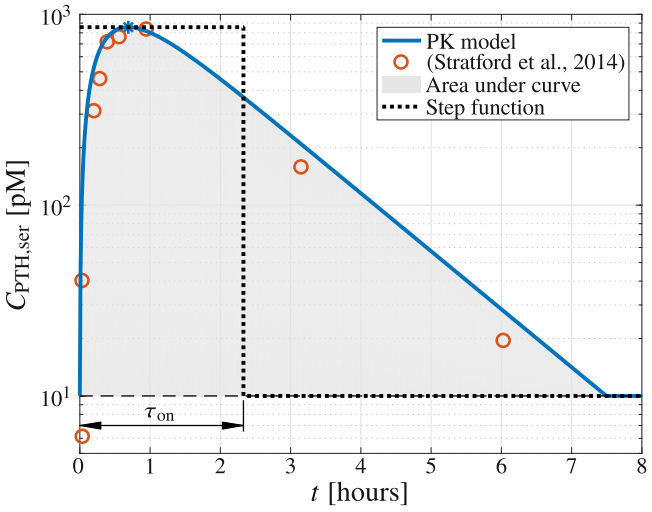

Fig. 2. Development of concentration of PTH(1-34) in serum over time, with the solid graph representing the PK model, and the circular markers representing the experimental data by Stratford et al. (2014). The grey area shows the area under the curve *AUC*, whereas the asterisk marker is C_{max}. The dotted graph shows the step function-representation of the PK model-derived serum concentration.

amount of drug that has already been systemically absorbed is the so-called area under the curve, standardly denoted as *AUC*, which is related to $C_{PTH,ser}$ via

$$\frac{dAUC}{dt} = C_{PTH,ser}\,. \tag{3}$$

Eqs. (1) to (3) can be solved analytically, giving access to mathematical expressions quantifying the time courses of $m_{PTH,sub}$ and $C_{PTH,ser}$, as well as to the *AUC*, in dependence of initial values $m_{PTH,sub}(t_0)$ and $C_{PTH,ser}(t_0)$, see Appendix B.

For the sake of demonstration, the PK model was applied in order to reproduce the experimentally measured serum concentrations of PTH(1-34) administered to rats, involving single doses of 80 µg/kg/day (Stratford et al., 2014). Remarkably, the latter dose is, in absolute terms, equivalent to the aforementioned dose of 20 µg/day that is used to treat PMO in women (considering that rats weigh, on average, 250 g). The PK parameters were deduced from data available in literature: $F = 0.95$ (Eli Lilly, 2014); $V_d = 3.52$ l, based on (Satterwhite et al., 2010); $k_a = 2.73$ 1/h and $k_e = 0.7$ 1/h, obtained from standard relations of pharmacokinetics based on data — namely, the point in time when $C^{max}_{PTH,ser}$ is reached and the terminal half-life of PTH(1-34) — accessible in (Stratford et al., 2014). Considering furthermore the aforementioned dose in terms of a corresponding initial condition for the mass of PTH(1-34) in the subcutaneous tissue, $m_{PTH,sub}(t_0) = 20$ µg, and that initially $C_{PTH,ser}$ is equal to the background concentration of PTH, $C^{back}_{PTH,ser}$, which is known to amount to 10 pM (Stratford et al., 2014), hence $C_{PTH,ser}(t_0) = C^{back}_{PTH,ser} = 10$ pM, gives access to the drug concentration-versus-time plot, see Fig. 2. The (blue) solid line represents the development over time of the serum drug concentration, whereas the (red) circle-shaped markers represent the experimental data provided by Stratford et al. (2014). Clearly, the model-predicted serum concentration of PTH(1-34) agrees well the experimental data, corroborating the validity of the PK model. Furthermore, the (blue) asterisk-shaped marker represents the maximum drug concentration $C^{max}_{PTH,ser}$, which the PK model predicts to occur 41.34 min after drug administration This result also aligns well with the observations reported by Stratford et al. (2014).

In the mechanistic PK/PD model elaborated in Section 2.3, the variation over time of the drug concentration is used as external stimulus controlling the activity of bone cells. In order to distinguish between continuous and intermittent PTH(1-34) stimuli, leading to different cellular behaviours, the PK model-derived function $C_{PTH,ser}(t)$ was approximated in terms of an equivalent step function (Potter et al., 2005). The latter was chosen such that the *AUC* computed with the PK model, by means of Eq. (27), was preserved (Fletcher et al., 2014). As for intermittent administration, the frequency of the step function amounts to 24 h, which is split up into a period τ_{on} during which the concentration is fixed at $C^{max}_{PTH,ser}$, and a period τ_{off} during which the concentration is fixed at $C^{back}_{PTH,ser}$, with $\tau_{on} + \tau_{off} = 24$ h. For defining the actual value of τ_{on}, the requirement was considered that the exact function of $C_{PTH,ser}(t)$ and the corresponding step function must exhibit the same *AUC*. Knowing the latter from integration of Eq. (3), as well as the amplitude of the step function, which amounts to $\left(C^{max}_{PTH,ser} - C^{back}_{PTH,ser}\right)$, τ_{on} follows as

$$\tau_{on} = \frac{AUC}{C^{max}_{PTH,ser} - C^{back}_{PTH,ser}}. \tag{4}$$

In the present case, the area under the curve amounts to $AUC = 1971.11$ pM h, and the maximum serum concentration amounts to $C^{max}_{PTH,ser} = 856.42$ pM; hence $\tau_{on} = 2.33$ h, see the respective graph indicated in Fig. 2. Notably, the step function representation of the serum concentration of PTH(1-34) was preferred merely for the sake of better practicability, as compared to using directly the exact time course $C_{PTH,ser}(t)$.

2.2. Effect of PTH(1-34) administration on the overall PTH concentration

As is explained in detail in Section 2.3, the mechanistic PK/PD model presented in this paper is regulated by the current concentration of PTH (among other factors). The actual implementation of PTH in the model is based on a number of assumptions and considerations — clearly summarising those is the focus of this section.

First of all, no distinction is made between endogenously produced PTH and PTH(1-34) administered through (intermittent) subcutaneous injections or (continuous) intravenous infusions. If no external dosage of PTH(1-34) occurs, the concentration of PTH available to bone cells and other factors equals the so-called background concentration, $C_{PTH,ser} = C^{back}_{PTH,ser}$. For humans, $C^{back}_{PTH,ser}$ amounts to 3 pM (Satterwhite et al., 2010), whereas for rats, it amounts to 10 pM (Stratford et al., 2014). Upon intermittent administration of PTH(1-34), the concentration of PTH is set to the peak concentration, $C_{PTH,ser} = C^{max}_{PTH,ser}$, whereby $C^{max}_{PTH,ser}$ is determined as shown in Section 2.1. After a time period of τ_{on}, the pulsatile, stepwise stimulus of PTH ends, and $C_{PTH,ser}$ is set back to $C^{back}_{PTH,ser}$. As for continuous administration of PTH(1-34), we have adapted the PK model presented in Section 2.1 in a suitable way, and considered a dosage of 40 µg/kg/day, according to the study of Li et al. (2007), see also Section 2.5.

Finally, it is noted that while up to this point the serum concentration of PTH has been denoted as $C_{PTH,ser}$, we use, for the sake of conciseness, C_{PTH} subsequently.

2.3. Mathematical model relating PTH administration to bone cell activities

2.3.1. Bone cell population model of bone remodelling and bone modelling

The starting point for the subsequently elaborated PD model, which allows for estimation of the bone cell activity-related effects PTH administration entails, was the BCPM going back to the

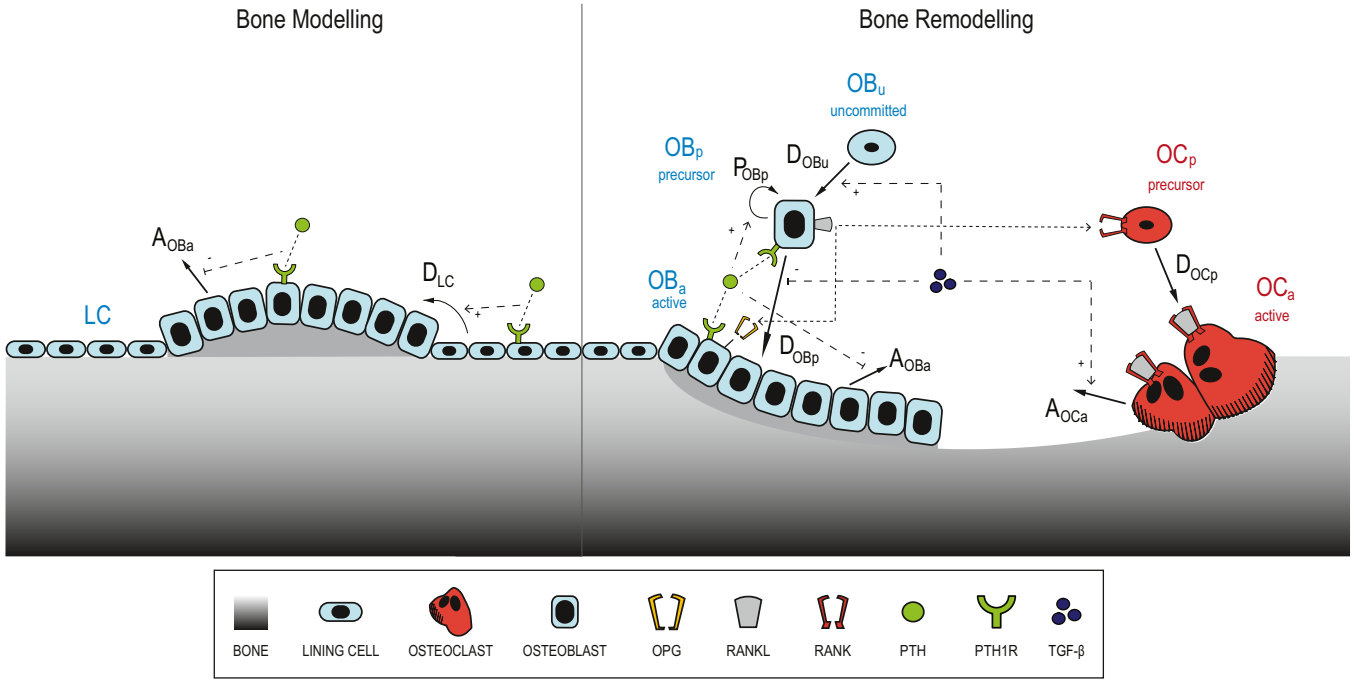

Fig. 3. Schematic illustration of the BCPM, distinguishing between bone modelling and bone remodelling, including the involved regulatory mechanisms (RANK-RANKL-OPG pathway, TGF-β and PTH). The osteoblastic lineage includes osteoblast progenitors, precursors, active cells, and lining cells; whereas the osteoclastic lineage includes precursors and active cells.

seminal contribution of Lemaire et al. (2004), which was later refined and extended by Pivonka and co-workers (Pivonka et al., 2008; 2010; Scheiner et al., 2013; Pivonka et al., 2013; Pastrama et al., 2018). The key novelties of the new model formulation comprise consideration of bone modelling effects, as well as new, PTH administration-specific regulatory mechanisms, see Fig. 3 for a respective illustration.

One of the main features of BCPMs is the consideration of bone cells in terms of molar concentrations (instead of cell numbers). Inspired by the aforementioned works, the kinetic equations describing mathematically how the concentrations of the cells involved in bone remodelling change are defined as follows:

$$\frac{dC_{OBP}}{dt} = \mathcal{D}_{OBU}\,\pi^{\text{TGF-}\beta}_{act,OBU}\,C_{OBU} + \mathcal{P}_{OBP}\,H^{+}_{PTH,\mathcal{P}_{OBP}}\,C_{OBP} - \mathcal{D}_{OBP}\,\pi^{\text{TGF-}\beta}_{rep,OBP}\,C_{OBP}, \tag{5}$$

$$\frac{dC_{OBA/r}}{dt} = \mathcal{D}_{OBP}\,\pi^{\text{TGF-}\beta}_{rep,OBP}\,C_{OBP} - \mathcal{A}_{OBA}\,H^{-}_{PTH,\mathcal{A}_{OBA}}\,C_{OBA/r}\,, \tag{6}$$

and

$$\frac{dC_{OCA}}{dt} = \mathcal{D}_{OCP}\,\pi^{\text{RK-RKL}}_{act,OCP}\,C_{OCP} - \mathcal{A}_{OCA}\,\pi^{\text{TGF-}\beta}_{act,OCP}\,C_{OCA}\,. \tag{7}$$

In Eqs. (5) to (7), C_{OBU}, C_{OBP}, $C_{OBA/r}$, C_{OCP}, and C_{OCA} denote the concentrations of uncommitted osteoblast progenitors, of osteoblast precursors, of active osteoblasts that have differentiated in the course of the bone remodelling process, of osteoclast precursors, and of active osteoclasts; $\mathcal{D}_{OBP}$, $\mathcal{D}_{OBU}$, and $\mathcal{D}_{OCP}$ denote the maximum differentiation rates of uncommitted osteoblast progenitors, of osteoblast precursors, and of osteoclast precursors; $\mathcal{P}_{OBP}$ denotes the baseline proliferation rate of osteoblast precursors; while $\mathcal{A}_{OBA}$ and $\mathcal{A}_{OCA}$ denote the baseline apoptosis rate of active osteoblasts and the maximum apoptosis rate of active osteoclasts. Following numerous experimental studies, the differentiation, proliferation, and apoptosis processes included in Eqs. (5) to (7), are regulated by the presence of transforming growth factor (TGF-β), of free ligands (RANKL) of the receptor activator nuclear factor κB (RANK), which is also influenced by osteoprotegerin (OPG) in the framework of the RANK-RANKL-OPG pathway, as well as of systemically produced and administered PTH — see Pivonka et al. (2008) for a respective literature review — all of which are considered by corresponding regulatory functions. In particular, $\pi^{\text{TGF-}\beta}_{act,OBU}$, $\pi^{\text{TGF-}\beta}_{rep,OBP}$, $\pi^{\text{RK-RKL}}_{act,OCP}$, and $\pi^{\text{TGF-}\beta}_{act,OCP}$ are Hill-type functions which are assumed to vary between 0 and 1, and which depend on the current concentrations of TGF-β and of the RANK-RANKL complexes. Details on the definition of those functions are provided in Section 2.3.3 of this paper. Furthermore, $H^{+}_{PTH,\mathcal{P}_{OBP}}$ and $H^{-}_{PTH,\mathcal{A}_{OBA}}$ are so-called sigmoid E_{max} functions taking into account the regulatory effect of PTH on the proliferation of osteoblast precursors, and on the apoptosis of active osteoblasts, see Section 2.3.4 for further details.

As compared to previous model formulations, (Pivonka et al., 2008; 2010), one additional ODE has been considered in this work, accounting for bone modelling, namely

$$\frac{dC_{OBA/m}}{dt} = \mathcal{D}_{LC}\,H^{+}_{PTH,D_{LC}}\,C_{LC} - \mathcal{A}_{OBA}\,H^{-}_{PTH,\mathcal{A}_{OBA}}\,C_{OBA/m}\,, \tag{8}$$

where $C_{OBA/m}$ is the concentration of active osteoblasts that have differentiated in the course of the bone modelling process, C_{LC} is the (constant) concentration of lining cells, $\mathcal{D}_{LC}$ is the baseline differentiation rate of lining cells, and $\mathcal{A}_{OBA}$ is the baseline apoptosis rate of active osteoblasts which has already occurred in Eq. (6). Eq. (8) takes into account that also the differentiation of lining cells is regulated by PTH, via regulatory function $H^{+}_{PTH,D_{LC}}$.

2.3.2. Link between bone cell activities and bone composition change

Following the approach used in previous studies (Pivonka et al., 2012; Scheiner et al., 2013), bone is considered to be a two-phase material formed of extravascular bone matrix and vascular pore spaces. Thereby, the two constituents are quantified based on volume fractions; f_{bm} denotes the volume fraction of bone matrix, whereas f_{vas} denotes the volume fraction of vascular pore space, $f_{bm} + f_{vas} = 1$. The temporal development of the bone volume fraction is modelled via one ODE taking into account the amounts of

bone removed and formed over time, reading as

$$\frac{\mathrm{d}f_{\mathrm{bm}}}{\mathrm{d}t} = -\mathcal{K}_{\mathrm{res}}\, C_{\mathrm{OCA}} + \mathcal{K}_{\mathrm{form}}\,(C_{\mathrm{OBA/r}} + C_{\mathrm{OBA/m}})\,, \tag{9}$$

where $\mathcal{K}_{\mathrm{res}}$ and $\mathcal{K}_{\mathrm{form}}$, respectively, are the constant bone resorption and the constant bone formation rate, respectively. Notably, Eq. (9) is based on the assumption that the bone-forming capacities of active osteoblasts that have differentiated in the course of bone remodelling and those which have differentiated in the course of bone modelling are the same.

2.3.3. Regulatory effects of TGF-β and of the RANK-RANKL-OPG pathway

Following classical works on receptor-ligand binding kinetics as well as pertinent literature reviews, see, e.g., (Lauffenburger and Linderman, 1993; Pivonka et al., 2008), the Hill-type regulatory functions occurring in Eqs. (5) to (7) are defined as

$$\pi^{\text{TGF-}\beta}_{\mathrm{act,OBU}} = \pi^{\text{TGF-}\beta}_{\mathrm{act,OCP}} = \frac{C_{\text{TGF-}\beta}}{K^{\mathrm{act}}_{\text{TGF-}\beta} + C_{\text{TGF-}\beta}}\,, \tag{10}$$

$$\pi^{\text{TGF-}\beta}_{\mathrm{rep,OBP}} = \frac{K^{\mathrm{rep}}_{\text{TGF-}\beta}}{K^{\mathrm{rep}}_{\text{TGF-}\beta} + C_{\text{TGF-}\beta}}\,, \tag{11}$$

and

$$\pi^{\text{RK-RKL}}_{\mathrm{act,OCP}} = \frac{C_{\text{RK-RKL}}}{K^{\mathrm{act}}_{\text{RK-RKL}} + C_{\text{RK-RKL}}}\,, \tag{12}$$

where $C_{\text{TGF-}\beta}$ is the concentration of TGF-β, $C_{\text{RK-RKL}}$ is the concentration of the RANK-RANKL complex, $K^{\mathrm{act}}_{\text{TGF-}\beta}$ is the apparent dissociation equilibrium constant related to binding of TGF-β to its receptors on uncommitted osteoblast progenitors and active osteoclasts (interpretable as activation coefficient for the differentiations of osteoblast progenitors and active osteoclasts), $K^{\mathrm{rep}}_{\text{TGF-}\beta}$ is the apparent dissociation equilibrium constant related to binding of TGF-β to its receptors on osteoblast precursors (interpretable as repression coefficient for the differentiation of osteoblast precursors), and $K^{\mathrm{act}}_{\text{RK-RKL}}$ is the apparent dissociation equilibrium constant related to binding of RANK to RANKL (interpretable as activation coefficient for the differentiation of osteoclast precursors).

Evaluating Eqs. (10) to (12) necessitates definition of the included concentrations of TGF-β and of the RANK-RANKL complex. Furthermore, considering the regulatory pathways involved in the BCPM presented in Section 2.3.1, see (Pivonka et al., 2008) for a comprehensive summary, it turns out that in addition to $C_{\text{TGF-}\beta}$ and $C_{\text{RK-RKL}}$, also the concentrations of OPG, RANKL, the OPG-RANKL complex, and RANK must be defined. For that purpose, the principle of mass action kinetics is utilised, see (Pivonka et al., 2008; 2012) for details, yielding the following set of ODEs:

$$\frac{\mathrm{d}C_{\text{TGF-}\beta}}{\mathrm{d}t} = \alpha\, \mathcal{K}_{\mathrm{res}}\, C_{\mathrm{OCA}} + P^{\mathrm{d}}_{\text{TGF-}\beta} - D_{\text{TGF-}\beta}\, C_{\text{TGF-}\beta}\,, \tag{13}$$

where α is a constant quantifying how much TGF-β is released upon bone resorption, $P^{\mathrm{d}}_{\text{TGF-}\beta}$ is a term accounting for (external) dosage of TGF-β, and $D_{\text{TGF-}\beta}$ is the constant degradation rate of TGF-β;

$$\begin{aligned}\frac{\mathrm{d}C_{\mathrm{OPG}}}{\mathrm{d}t} &= \beta_{\mathrm{OPG}}\, C_{\mathrm{OBA}} \left(1 - \frac{C_{\mathrm{OPG}}}{C^{\mathrm{sat}}_{\mathrm{OPG}}}\right)\left(1 + \frac{C_{\mathrm{PTH}}}{K^{\mathrm{rep}}_{\mathrm{PTH}}}\right)^{-1} \\ &\quad - \left(D_{\mathrm{OPG}} + k^{\mathrm{f}}_{\text{OPG-RKL}}\, C_{\mathrm{RKL}}\right) C_{\mathrm{OPG}} \\ &\quad + P^{\mathrm{d}}_{\mathrm{OPG}} + k^{\mathrm{r}}_{\text{OPG-RKL}}\, C_{\text{OPG-RKL}},\end{aligned} \tag{14}$$

where C_{OPG} is the concentration of OPG, C_{RKL} is the concentration of RANKL, $C_{\text{OPG-RKL}}$ is the concentration of the OPG-RANKL complex, β_{OPG} is the intrinsic production rate of OPG, $C^{\mathrm{sat}}_{\mathrm{OPG}}$ is the saturation concentration of OPG, $K^{\mathrm{rep}}_{\mathrm{PTH}}$ is the apparent dissociation equilibrium constant related to binding of PTH to its receptors on osteoblast precursors and active osteoblasts (interpretable as repression coefficient for production of OPG), $P^{\mathrm{d}}_{\mathrm{OPG}}$ is a term accounting for (external) dosage of OPG, D_{OPG} is the constant degradation rate of OPG, and $k^{\mathrm{f}}_{\text{OPG-RKL}}$ and $k^{\mathrm{r}}_{\text{OPG-RKL}}$ are the association and dissociation rate constants quantifying the binding and debinding behaviour of OPG and RANKL;

$$\frac{\mathrm{d}C_{\text{OPG-RKL}}}{\mathrm{d}t} = k^{\mathrm{f}}_{\text{OPG-RKL}}\, C_{\mathrm{OPG}}\, C_{\mathrm{RKL}} - \left(k^{\mathrm{r}}_{\text{OPG-RKL}} + D_{\text{OPG-RKL}}\right) C_{\text{OPG-RKL}}, \tag{15}$$

where $D_{\text{OPG-RKL}}$ is the constant degradation rate of the OPG-RANKL complex;

$$\begin{aligned}\frac{\mathrm{d}C_{\mathrm{RKL}}}{\mathrm{d}t} &= \beta_{\mathrm{RKL}}\, C_{\mathrm{OBP}}\, \frac{C_{\mathrm{PTH}}}{\left(C_{\mathrm{PTH}} + K^{\mathrm{act}}_{\mathrm{PTH}}\right)} \times \left(1 - \frac{C_{\mathrm{RKL}} + C_{\text{OPG-RKL}} + C_{\text{RK-RKL}}}{N^{\mathrm{max}}_{\text{RANKL/OBP}}\, C_{\mathrm{OBP}}}\right) \\ &\quad + P^{\mathrm{d}}_{\mathrm{RKL}} - \left(k^{\mathrm{f}}_{\text{OPG-RKL}}\, C_{\mathrm{OPG}} + k^{\mathrm{f}}_{\text{RK-RKL}}\, C_{\mathrm{RK}} + D_{\mathrm{RKL}}\right) \\ &\quad \times C_{\mathrm{RKL}} + k^{\mathrm{r}}_{\mathrm{OPG}}\, C_{\text{OPG-RKL}} + k^{\mathrm{r}}_{\mathrm{RK}}\, C_{\text{RK-RKL}},\end{aligned} \tag{16}$$

where C_{RK} is the concentration of RANK, β_{RKL} is the intrinsic production rate of RANKL, $K^{\mathrm{act}}_{\mathrm{PTH}}$ is the apparent dissociation equilibrium constant related to binding of PTH to its receptors on osteoblast precursors and active osteoblasts (interpretable as activation coefficient for production of RANKL), D_{RKL} is the constant degradation rate of RANKL, $P^{\mathrm{d}}_{\mathrm{RKL}}$ is a term accounting for (external) dosage of RANKL, $N^{\mathrm{max}}_{\text{RANKL/OBP}}$ is the maximum amount of RANKL expressed by osteoblast precursors, and $k^{\mathrm{f}}_{\text{RK-RKL}}$ and $k^{\mathrm{r}}_{\text{RK-RKL}}$ are the association and dissociation rate constants quantifying the binding and debinding behaviour of RANK and RANKL;

$$\frac{\mathrm{d}C_{\text{RK-RKL}}}{\mathrm{d}t} = k^{\mathrm{f}}_{\text{RK-RKL}}\, C_{\mathrm{RK}}\, C_{\mathrm{RKL}} - \left(k^{\mathrm{r}}_{\text{RK-RKL}} + D_{\text{RK-RKL}}\right) C_{\text{RK-RKL}}, \tag{17}$$

where $D_{\text{RK-RKL}}$ is the constant degradation rate of the RANK-RANKL complex; and

$$\frac{\mathrm{d}C_{\mathrm{RK}}}{\mathrm{d}t} = P^{\mathrm{e}}_{\mathrm{RK}} + k^{\mathrm{r}}_{\text{RK-RKL}}\, C_{\text{RK-RKL}} - \left(k^{\mathrm{f}}_{\text{RK-RKL}}\, C_{\mathrm{RKL}} + D_{\mathrm{RK}}\right) C_{\mathrm{RK}}, \tag{18}$$

where $P^{\mathrm{e}}_{\mathrm{RK}}$ is the endogenous production rate of RANK, and D_{RK} is its constant degradation rate. Thereby, $P^{\mathrm{e}}_{\mathrm{RK}}$ is defined as $P^{\mathrm{e}}_{\mathrm{RK}} = N_{\text{RANK/OCP}}\, C_{\mathrm{OCP}}\, D_{\mathrm{RK}}$, with $N_{\text{RANK/OCP}}$ being the number of receptors per pM of osteoclast precursors, see Sections 3.1 and 3.2 of (Pivonka et al., 2012) for a detailed derivation of this definition. All parameters included in Eqs. (13) to (18) are defined in Appendix C, see Tables 3–8.

2.3.4. Regulatory effects of PTH

In our model, the anabolic effect of intermittent PTH administration is considered based on three mechanisms, see the corresponding literature review in Section 1 of this paper: (i) downregulation of active osteoblast apoptosis, (ii) upregulation of bone lining cell differentiation, and (iii) upregulation of osteoblast precursor proliferation.

Downregulation of active osteoblast apoptosis by PTH is considered as suggested by Peterson and Riggs (2010). Hence, the intracellular mechanism influencing the apoptosis pathway is assumed to be controlled by three regulatory factors, namely Runx2, CREB, and Bcl-2 (Bellido et al., 2003). Runx2 and phosphorylation of CREB (pCREB) are considered to be necessary for the transcription of the survival gene Bcl-2 and induce the anti-apoptotic effect on active osteoblasts. PTH is considered to act directly on the degradation of Runx2 in a fast and transient manner, whereas the production of pCREB occurs slower. Furthermore, Bcl-2 is considered to occur at intermediate speed, influenced by the developments of Runx2 and pCREB; hence, it is indirectly regulated by PTH. Bcl-2, in turn, is used as regulatory argument for the effect of PTH on active

Table 1
Regulatory factors regulating the intracellular signalling pathways involved in the anabolic response of bone tissue to intermittent PTH administration.

General parameter	Osteoblast apoptosis factor	Osteoblast precursor proliferation, lining cell differentiation factor
A	Runx2	Dvl
B	pCREB	Axin-APC-GSK-3 complex
G	Bcl-2	β-catenin

osteoblast apoptosis. In mathematical terms, the above-sketched mechanisms are captured based on three ODEs:

$$\frac{d\tilde{c}_A}{dt} = \tilde{\beta}_A - D_A\, H^+_{PTH,A}\, \tilde{c}_A\,, \tag{19}$$

$$\frac{d\tilde{c}_B}{dt} = \tilde{\beta}_B\, H^+_{PTH,B} - D_B\, \tilde{c}_B\,, \tag{20}$$

and

$$\frac{d\tilde{c}_G}{dt} = \tilde{\beta}_G\, \tilde{c}_A\, \tilde{c}_B - D_G\, \tilde{c}_G\,. \tag{21}$$

Thereby, it should be noted that subscript A represents Runx2, subscript B represents pCREB, and subscript G represents Bcl-2, see Table 1. Eqs. (19) to (21) are formulated in generalized notation, as these mechanisms are also utilised for describing mathematically the regulatory effects of intermittent PTH administration on osteoblast precursor proliferation, and lining cell differentiation, requiring ODEs which are formally identical (as explained in more detail later in this section). Furthermore, $\tilde{c}_A$, $\tilde{c}_B$ and $\tilde{c}_G$ are the concentrations of the involved factors — in the present case, the latter are Runx2, pCREB, and Bcl-2 — $\tilde{\beta}_A$, $\tilde{\beta}_B$, and $\tilde{\beta}_G$ are the corresponding intrinsic production rates, and D_A, D_B, and D_G the constant degradation rates. Notably, the concentrations and production rates are considered in terms of dimensionless numbers. This is due to the fact that those concentrations and production rates are not known, and the regulatory effects can be anyway sufficiently described based on the relative differences between the involved concentrations, production rates, and degradation rates. The initial conditions for the concentrations of the regulatory factors were chosen according to Peterson and Riggs (2010). Furthermore, the parameters occurring in Eqs. (19) to (21) were chosen based on the premise that intermittent and continuous administration of PTH can be clearly distinguished from each other, whereas experimentally based parameter fitting is not possible (due to the lack of suitable experimental data).

$H^+_{PTH,A}$ and $H^+_{PTH,B}$, occurring in Eqs. (19) and (20), are positive sigmoid E_{max} functions, driven by the concentration of PTH and accounting for its upregulating effect on the degradation of A and on the production of B, respectively; they are structured as follows:

$$H^+_{PTH,i} = \rho_i + \frac{(\alpha_i - \rho_i)\,(C_{PTH})^{\gamma_i}}{(\delta_i)^{\gamma_i} + (C_{PTH})^{\gamma_i}}\,, \tag{22}$$

where subscript i represents either factor A or factor B. The definition of $H^+_{PTH,i}$ includes quantity ρ_i, representing the baseline level of the function; i.e., if PTH is absent, then $H^+_{PTH,i} = \rho_i$. The baseline value of $H^+_{PTH,i}$ is considered to be related to the background concentration of PTH, as defined in Section 2.1. Furthermore, α_i is a parameter quantifying the maximum effect of PTH, δ_i is the potency of the response to drug administration (i.e., the concentration of PTH that causes 50% of the maximum effect), and γ_i is the steepness of the response — theoretically, the latter is related to the number of drug molecules combined with each receptor, but standardly it is used as phenomenological factor allowing for calibrating the model.

The anti-apoptotic effect of PTH on active osteoblasts is driven by the dimensionless concentration of Bcl-2, $\tilde{c}_{Bcl\text{-}2}$, which is represented in the general notation of Eqs. (19) to (21) by $\tilde{c}_G$. In order to describe this mechanism mathematically, a corresponding negative sigmoid E_{max} function is used, see Eqs. (6) and (8), reading as

$$H^-_{PTH,\mathcal{A}_{OBA}} = \alpha_{\mathcal{A}_{OBA}} - \frac{(\alpha_{\mathcal{A}_{OBA}} - \rho_{\mathcal{A}_{OBA}})\,(\tilde{c}_{Bcl\text{-}2})^{\gamma_{\mathcal{A}_{OBA}}}}{(\delta_{\mathcal{A}_{OBA}})^{\gamma_{\mathcal{A}_{OBA}}} + (\tilde{c}_{Bcl\text{-}2})^{\gamma_{\mathcal{A}_{OBA}}}}\,, \tag{23}$$

where the physical meaning of the involved parameters is as explained below Eq. (22). For determining the value of the potency $\delta_{\mathcal{A}_{OBA}}$, a baseline value of the sigmoid function of $H^-_{PTH,\mathcal{A}_{OBA}} = 1$ was considered. Inserting then the numerical values of all other parameters gives access to the numerical value of $\delta_{\mathcal{A}_{OBA}}$, see Table 7.

The action of PTH on the proliferation of osteoblast precursors as well as on the differentiation of lining cells takes into account the canonical Wnt pathway, which plays an essential role in many aspects of cell growth, proliferation and differentiation (Fuerer et al., 2008). Given the importance of Wnt signalling in embryonic development and carcinogenesis, numerous computational models simulating the complex intracellular transduction mechanisms have been developed. However, the multitude of transmembrane ligands and receptors involved made it difficult to distinguish the action of PTH on each individual component. Since the development of a complex model dealing with intracellular Wnt signalling is beyond the scope of this paper, a more phenomenological strategy was pursued, considering the components in this pathway in simplified manner. In particular, three components were accounted for: (i) Dishevelled (Dvl), (ii) Axin-APC-GSK-3 complex, (iii) β-catenin. Furthermore, it is assumed that intermittent PTH administration transiently degrades Dvl, while the involved characteristic time corresponds to the characteristic time of PTH administration. The production rate of the Axin-APC-GSK-3 complex is assumed to be regulated by PTH, while the production dynamics is slower than the dynamics related to the effects of Dvl. Finally, the β-catenin concentration is assumed to be proportional to the Dvl and Axin-APC-GSK-3 complex concentrations, and subjected to a first-order degradation rate. The development of the β-catenin level is used as regulatory factor for the effect of PTH on osteoblast precursor proliferation and on lining cell differentiation. For that purpose, the three general ODEs defined in Eqs. (19) to (21) are utilised, with factor A representing Dvl, factor B representing the Axin-APC-GSK-3 complex, and factor C representing β-catenin, see Table 1. The two positive sigmoid E_{max} functions co-regulating Eqs. (5) and (8), driven by the β-catenin concentration, are defined:

$$H^+_{PTH,i} = \rho_i + \frac{(\alpha_i - \rho_i)\,(\tilde{c}_{\beta\text{-}cat})^{\gamma_i}}{(\delta_i)^{\gamma_i} + (\tilde{c}_{\beta\text{-}cat})^{\gamma_i}}\,, \tag{24}$$

with subscript i representing either the proliferation rate of osteoblast precursors, $\mathcal{P}_{OBP}$, or the differentiation rate of lining cells, $\mathcal{D}_{LC}$. $\tilde{c}_{\beta\text{-}cat}$ denotes the concentration of β-catenin.

Remarkably, the same model parameters were used for calculation of $\tilde{c}_{Bcl\text{-}2}$ and $\tilde{c}_{\beta\text{-}cat}$, entering the system of ODEs defined by Eqs. (19) to (21). Also the same initial conditions were applied. However, the sigmoid E_{max} functions fed by $\tilde{c}_{Bcl\text{-}2}$ and $\tilde{c}_{\beta\text{-}cat}$, respectively, Eqs. (23) and (24) are calibrated individually for the targeted effects, according to experimental data.

2.3.5. Model summary

The mathematical framework defining the extended BCPM consists of a system of ODEs, namely of Eqs. (5) to (9), (13) to (18), and (19) to (21), as well as the regulatory functions defined in Eqs. (10) to (12), and (22) to (24). For numerical solution of this system of equations, the commercial software Matlab has been utilised, in particular one of the solvers (ode45) provided for numerical integration of ODE systems. Thereby, it should be noted that, in contrast to previous model formulations (Pivonka et al., 2008; 2010), all regulatory functions had to be explicitly expressed in the ODE system, and solved simultaneously with the

aforementioned set of ODEs. All model parameters are summarised in Appendix C, see Tables 3–8.

2.4. Mechanism to simulate OVX

According to experimental observations, both osteoporosis in humans and OVX in animals are associated with a disturbance of the RANK-RANKL-OPG pathway, leading to an increased RANKL/OPG ratio (Hofbauer et al., 2004). In the mechanistic PK/PD model, this effect can be taken into account through imposing a corresponding increase in the RANKL concentration, which consequently induces a catabolic action on bone. To that end, Eq. (16), which describes the dynamics of the RANKL concentration, includes the dosage term $P^{\mathrm{d}}_{\mathrm{RKL}} = P^{\mathrm{OVX}}_{\mathrm{RKL}}$, taking into account a constant, OVX-related RANKL production.

2.5. Experimental data for model calibration and validation

Four independent experimental data sets were considered for calibrating and validating the mechanistic PK/PD model, described below. Notably, all of the considered studies were conducted on 3-month-old, Sprague-Dawley female rats, weighing between 220 and 250 g. Furthermore, the development of the condition of the rats during the experiments was quantified in terms of the BV/TV (i.e., the ratio of bone volume over total volume), which is equivalent to the bone tissue volume fraction f_{bm}, the latter being one of the state variables of the mechanistic PK/PD-model, see, e.g., Eq. (9). Notably, in three of the below described experimental studies, the BV/TV was measured in the trabecular tissue in the proximal tibial metaphysis (Wronski et al., 1988; Liu and Kalu, 1990; Wronski and Dann, 1993), while in one study the trabecular tissue in the proximal femoral metaphysis was considered (Li et al., 2007).

Li et al. (2007) investigated the dual action of intermittent and continuous administration of synthetic human PTH(1-34) to healthy rats. The administration was maintained for 14 days, involving both daily (i.e., intermittent) subcutaneous injections at a dose of 80 μg/kg/day and continuous infusion at a dose of 40 μg/kg/day. Li et al. (2007) revealed that after 14 days of intermittent administration of PTH(1-34), the BV/TV amounted to $29.1 \pm 2.8\%$, while the respective control BV/TV amounted to $23.8 \pm 2.4\%$; hence, an increase in BV/TV by $5.3 \pm 3.7\%$ was observed. After 14 days of continuous administration of PTH(1-34), in turn, the BV/TV amounted to $14.8 \pm 1.0\%$, while the respective control BV/TV amounted to $20.6 \pm 1.0\%$; hence, a decrease in BV/TV by $5.8 \pm 1.4\%$ was observed.

Wronski et al. (1988) studied the reduction of the BV/TV during 100 days after the rats had undergone sham surgery or ovariectomy. In particular, after sham surgery, the BV/TV amounted to 27.3 ± 5.0 %. This value was considered as baseline value. Wronski et al. (1988) measured then the BV/TV 14, 35, 52, 70, and 100 days after ovariectomy, amounting to $21.1 \pm 6.8\%$, $16.1 \pm 4.7\%$, $11.9 \pm 4.3\%$, $11.6 \pm 6.5\%$, and $5.5 \pm 3.3\%$.

Liu and Kalu (1990) investigated the change in BV/TV 35 days after sham surgery, after ovariectomy without treatment by PTH(1-34), as well as after ovariectomy directly followed by intermittent administration of PTH, considering thereby two different doses, namely 80 μg/kg/day and 160 μg/kg/day. After sham surgery, which is again considered as reference in this study, the BV/TV amounted to $25.2 \pm 1.6\%$, and after ovariectomy to $12.6 \pm 1.8\%$. When intermittently administering PTH(1-34) at a dose of 80 μg/kg/day, the BV/TV amounted to $60.2 \pm 2.9\%$, while doubling the dose led to a further increase in BV/TV to $70.1 \pm 2.3\%$.

The fourth study considered for model calibration and validation, respectively, was carried out by Wronski and Dann (1993). They performed both sham surgery and ovariectomy on the aforementioned type of rats, and considered a resting phase of 28 days before measurements were conducted and/or administration of PTH(1-34) was initiated. Directly after this resting phase, as well as on days 63 and 98 after surgery, they measured the BV/TV of rats which have undergone sham surgery, of OVX rats which did not receive any drug treatment, and of OVX rats which received intermittent administration of PTH(1-34), at a dose of 80 μg/kg/day. The animals which underwent sham surgery showed a more or less constant BV/TV over time, amounting on average to $27.1 \pm 1.2\%$ (measured at day 63 after surgery). The OVX rats exhibited a BV/TV-development reading as $9.0 \pm 1.8\%$ at day 28, $4.2 \pm 1.1\%$ at day 63, and $4.0 \pm 1.0\%$ at day 98 after ovariectomy. If treated intermittently by PTH(1-34), the BV/TV of the rats evolved as follows: it amounted to $8.9 \pm 1.8\%$ at day 28, $27.0 \pm 3.8\%$ at day 63, and $53.7 \pm 4.5\%$ at day 98 after ovariectomy.

3. Results

First, calibration of the mechanistic PK/PD model needed to be performed. As for the model parameters related to administration of PTH(1-34), the experimental results published by Li et al. (2007), see Section 2.5, were considered for that purpose. Thereby, the focus was on intermittent administration of PTH(1-34), in terms of achieving the best-possible agreement between model predictions and experimental data. When simulating intermittent administration of PTH(1-34) for 14 days, the increase of the trabecular bone volume fraction f_{bm} (which is equivalent to the BV/TV) amounted to 5.5%, with respect to baseline. This result is in good agreement with the corresponding experimental result of $5.3 \pm 3.7\%$ (Li et al., 2007), see Fig. 4(a). When simulating, again for 14 days, continuous administration of PTH(1-34), the model predictions exhibit the desired catabolic behaviour, reflected by decrease of the trabecular bone volume fraction. However, our model predicts a decrease in f_{bm} of 1.4%, whereas the corresponding experimental study shows a reduction by $5.8 \pm 1.4\%$, see Fig. 4(b). Hence, our model seems to underestimate the catabolic effect of

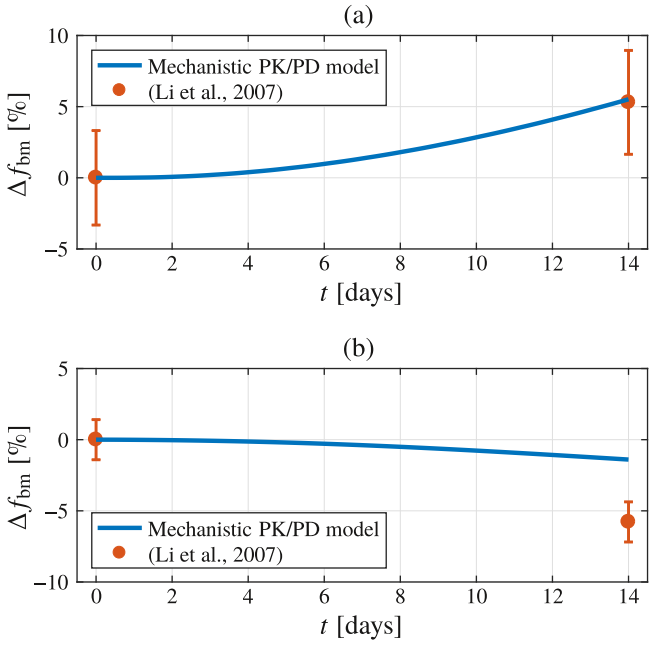

Fig. 4. Results of model calibration in terms of the change in trabecular bone volume fraction f_{bm} over time (with respect to baseline), following 14 days of (a) intermittent and (b) continuous administration of PTH(1-34) in a healthy rat model.

continuous administration of PTH(1-34). Nevertheless, since the main priority of the study presented in this paper was to reliably predict the effect of intermittent administration of PTH(1-34), the results of this calibration step were considered for further computations.

In a second step of model calibration, the OVX-related RANKL-production term, P_{RKL}^{OVX}, had to be defined, see Section 2.4. This was done based on data related to OVX rats which were not subjected to any kind of treatment by PTH(1-34) (Wronski et al., 1988). For $P_{RKL}^{OVX} = 416.7\,\text{pM/h}$, the model predictions show a satisfying agreement with the experimental data provided by Wronski et al. (1988), see Fig. 5. Within the first 60 days of simulated OVX, bone loss due to OVX occurs at a high rate, with the reduction of f_{bm} amounting to $\approx$15% (from an initial value of $\approx$25%). After day 60, bone loss slows down significantly (about 2 orders of magnitude). In fact, the bone loss rate reduces from 0.012%/day to 0.00081%/day, reaching eventually a quasi-stable state at a trabecular bone volume fraction of $\approx$5%.

Validation was performed, on the one hand, through comparison of the OVX simulation shown in Fig. 5 to the corresponding data by Wronski and Dann (1993). Clearly, the BV/TV-values provided by Wronski and Dann (1993) are lower than the model-predicted ones. Nevertheless, between 28 and 63 days after ovariectomy, the data of Wronski and Dann (1993) exhibits a bone loss rate which is quite similar to the model-predicted one, whereas later the experimental data seems to converge to the model predictions. Furthermore, treatment of OVX rats by PTH(1-34) was simulated, accounting thereby for two different drug doses (80 and 160 µg/kg/day) and two different treatment starting points (both directly after ovariectomy and considering a delay of 28 days). Considering again also the case where no drug treatment was performed, a good agreement between model predictions and the experimental data of (Liu and Kalu, 1990) was observed after 35 days. The model predictions showed a reduction in f_{bm} by $\approx$10 %, see Fig. 6, whereas the corresponding experimentally revealed reduction amounted to 12.6 ± 2.4% (Liu and Kalu, 1990). Simulating treatment by PTH(1-34) starting directly after the ovariectomy, the following change of the f_{bm} (with respect to baseline) turned out to increase non-linearly with increasing doses. Doubling the dose from 80 µg/kg/day to 160 µg/kg/day, a 1.3-fold increase of the drug effects is observed, see Fig. 6; this is in good

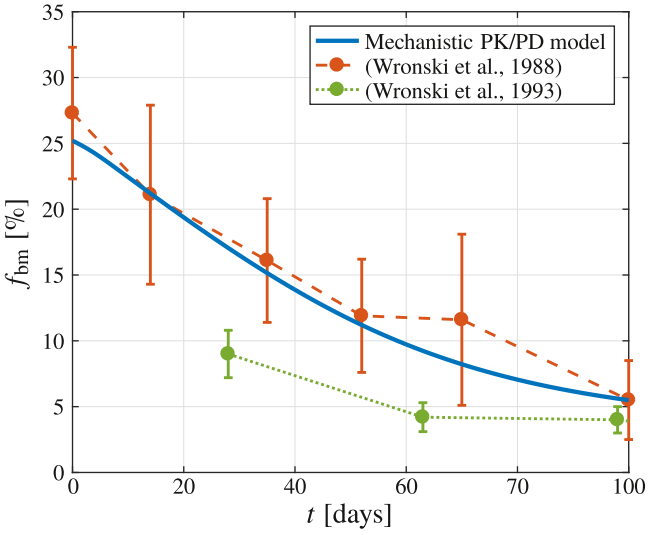

Fig. 5. Model-predicted versus experimentally observed changes in the trabecular bone volume fraction f_{bm} in the course of 100 days after ovariectomy in a rat model of osteoporosis. The data in (Wronski et al., 1988) were used for model calibration, whereas the data in (Wronski and Dann, 1993) were used for model validation.

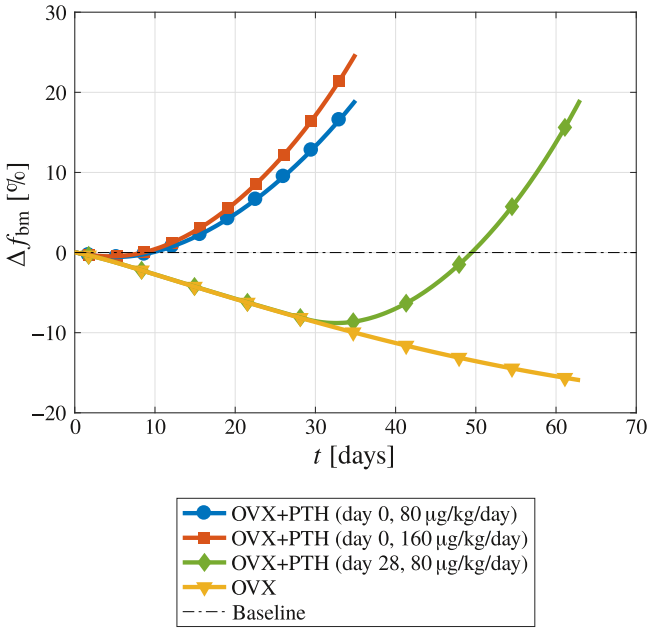

Fig. 6. Change of f_{bm} over time (with respect to baseline) resulting from simulations of OVX and treatment with intermittent administration of PTH(1-34) in a rat model of osteoporosis.

agreement with the corresponding experimental results, showing a 1.29-fold increase (Liu and Kalu, 1990). The model-predicted bone gain (with respect to baseline) computed when simulating a delay of 28 days between ovariectomy and treatment initiation amounts to $\approx$19 % at day 63, see Fig. 6. This value is much higher than the corresponding experimental result published by Wronski and Dann (1993) which suggests that at this point in time the BV/TV has just returned to baseline. However, when considering only the relative change between 28 and 35 days, in terms of a ratio defined as $[\Delta f_{bm}(t = 63\text{ days}) - \Delta f_{bm}(t = 28\text{ days})]/f_{bm}(t = 28\text{ days})$, this relative change ratio amounts to 1.6 according to the model predictions, whereas it amounts to 2.0 according to the experimental data of Wronski and Dann (1993). Hence, in terms of relative changes, the agreement between model predictions and experimental data can be considered satisfying.

Next, the effects of intermittent administration of PTH(1-34) on the regulatory factors controlling the intracellular signalling pathways driving the anabolic action that PTH(1-34) exerts on bone tissue are shown in Fig. 7. Fig. 7(a) shows how the serum concentration of PTH varies over time in response to daily subcutaneous injections. Fig. 7(b) shows the corresponding time course of the dimensionless concentration of regulatory factor A. Similarly to PTH, factor A is characterised by fast dynamics, see Eq. (19), implying that is follows variations of the PTH concentration quickly. Furthermore, the simulations show that within 11 h after drug administration, the value of factor A returns to the baseline value. In Fig. 7(c), the development of the dimensionless concentration of regulatory factor B, which is characterised by slow dynamics, see Eq. (20), is depicted. As a consequence of its dynamics, factor B reacts slowly to administration of PTH(1-34). Hence, while an injection of PTH(1-34) leads to a quasi-instantaneous increase of C_B, followed by a slowly progressing decrease, C_B does not return to the baseline. Instead, a long-term accumulation of factor B is observed. Finally, the temporal development of the dimensionless concentration of regulatory factor G over the simulated period of intermittent PTH(1-34) administration is plotted, see Fig. 7(d). Notably, factor G is

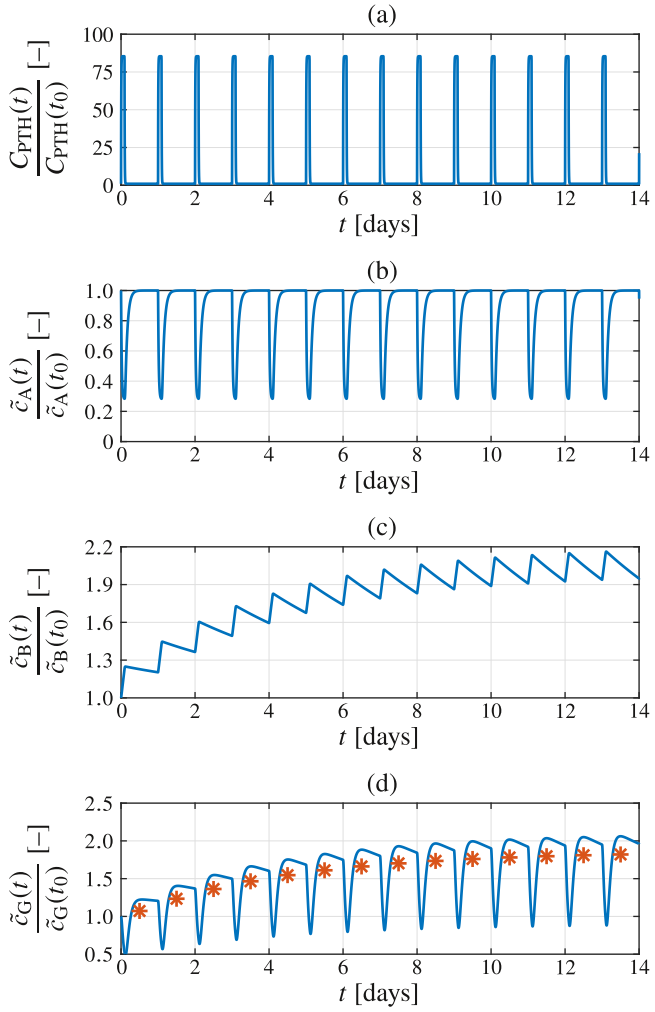

Fig. 7. Developments over time of (a) the concentration of PTH, C_{PTH}; (b) the dimensionless concentration of regulatory factor A, $\tilde{c}_A$; (b) the dimensionless concentration of regulatory factor B, $\tilde{c}_B$; and (b) the dimensionless concentration of regulatory factor G, $\tilde{c}_G$; in response to intermittent administration of PTH(1-34) at a dose of 80 µg/kg/day. All concentrations are normalised by the respective baseline values. The asterisk markers in (d) represent the daily averages of the normalised concentration of regulatory factor G.

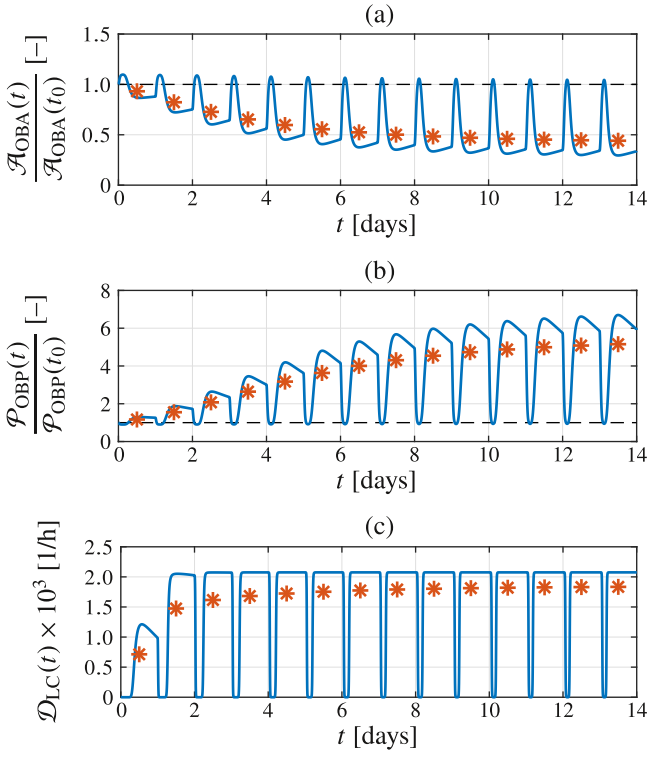

Fig. 8. Developments over time of (a) the apoptosis rate of active osteoblasts, $\mathcal{A}_{OBA}$; (b) the proliferation rate of osteoblast precursors, $\mathcal{P}_{OBP}$; and (c) the differentiation rate of lining cells, $\mathcal{D}_{LC}$; in response to intermittent administration of PTH(1-34) at a dose of 80 µg/kg/day. The asterisk markers represent the daily averages of the plotted quantities.

characterised by moderately fast dynamics, see Eq. (21), which is clearly reflected by the corresponding time course of C_G.

Interestingly, factor G, whose dependance on intermittent administration of PTH(1-34) is described in the previous paragraph, is used to control the regulatory functions which influence the apoptosis rate of active osteoblasts, $\mathcal{A}_{OBA}$, the proliferation rate of osteoblast precursors, $\mathcal{P}_{OBP}$, and the differentiation rate of lining cells, $\mathcal{D}_{LC}$, see Eqs. (6), (5), and (8) for the respective functional relations. Hence, driven by the time course of the concentration of regulatory factor G, occurring in response to administration of PTH(1-34), see Fig. 7(d), $\mathcal{A}_{OBA}$, $\mathcal{P}_{OBP}$, and D_{LC} change over time as well. The time courses of these quantities are shown in Fig. 8. Considering the average concentrations per administration interval (indicated by the red markers in Fig. 8), it is noted that, according to the mechanistic PK/PD model, $\mathcal{A}_{OBA}$ reduces by $\approx$50 % (with respect to baseline), see Fig. 8(a), whereas $\mathcal{P}_{OBP}$ increases by factor $\approx$5 (with respect to baseline), see Fig. 8(b). It is also worth mentioning that, since the differentiation of lining cells is a process which is fundamentally activated by intermittent administration of PTH(1-34), no baseline for the lining cell differentiation rate can be defined, because of which the time course of $\mathcal{D}_{LC}$ is plotted in terms of absolute values (instead of normalised ones), see Fig. 8(c).

4. Discussion

The results presented in Section 3 clearly show that the new mechanistic PK/PD model proposed in this paper is indeed able to reproduce both anabolic and catabolic responses bone cell responses, depending on whether PTH(1-34) is administered intermittently or continuously. It should be noted that to that end, the (anabolic) osteoblast proliferation-related term of the model needs to be sufficiently small (in magnitude), in order to ensure that the dual action of PTH(1-34) can be reproduced (Buenzli et al., 2012); if this term is too large, it would overwrite the effects of the catabolic pathways of the model. Furthermore, the introduction of the bone modelling process in the BCPM has turned out to be essential for simulating the partly substantial bone loss and gain reported in previous studies on rat models which have undergone ovariectomy and/or administration of PTH(1-34). This is in agreement with data from literature suggesting that, in rats, the bone modelling response to intermittent PTH(1-34) administration is an important mechanism as to how PTH(1-34) exerts its anabolic action. A recent lineage tracing study in mice using an inducible gene system that labelled mature osteoblasts also confirmed that PTH(1-34) can re-activate lining cells (Kim et al., 2012). In particular, in PTH(1-34)-treated animals, labelled cuboidal cells (active osteoblasts) were detected on the periosteal surface of bone, whereas in vehicle-treated animals, labelled cells appeared flat (lining cells). Moreover, compared to baseline, PTH(1-34) treatment increased by 50% the thickness of osteoblast-like cells in the calvaria and at the tibial periosteum.

Simulating intermittent administration of PTH(1-34) by means of the mechanistic PK/PD model presented in this paper yielded model predictions which are, at least partly, in good agreement with corresponding experimental data. It turned out that the model could be calibrated such that the bone gain reported when PTH(1-34) is administered intermittently, can be predicted very accurately. In contrast, the model appears to be not able to reproduce the quite significant bone loss due to continuous administration of PTH(1-34) over a period of 14 days, as reported in literature (Li et al., 2007). Nevertheless, in qualitative terms, the catabolic response of bone tissue to continuous administration of PTH(1-34) administration can be clearly recognised in the model predictions. Furthermore, the model turned out to be capable of reproducing the non-linear dependency of the bone gain on the dose administered — doubling the dose induced an increase in bone gain of approximately 30%. Our model is also able to reproduce some characteristics of different intermittent administration regimes of PTH(1-34), considering OVX rats, see Section 3. Interestingly, simulating intermittent administration of PTH(1-34) at a dose of 80 μg/kg/day to OVX rats showed a slower bone gain as compared to healthy animals. In particular, simulating 14 days of treatment, the model-predicted bone gain was by approximately 50% lower in OVX rats, compare Figs. 4(a) and 6. Clearly, this behaviour can be explained by the catabolic effect of ovariectomy.

Considering the results of Wronski and Dann (1993), who studied the effect of intermittent PTH(1-34) administration in OVX rats whereby the treatment was initiated with delay of 28 days after the ovariectomy, the model predictions are in good agreement with the experimental data, in terms of the relative change in the bone volume fraction. as presented in detail in Section 3. However, our model consistently overestimates the bone volume fraction, as compared to the results of Wronski and Dann (1993). On the other hand, considering now the study of Liu and Kalu (1990), our model adequately reproduces the non-linear dependency of the drug effect (in terms of increase in f_{bm} or BV/TV, respectively) on the administered dose, whereas the model-predicted bone gain is less substantial than observed in the experimental study published by Liu and Kalu (1990). Hence, the model predictions somehow span a bridge between the significantly varying experimental results. These discrepancies may also indicate that further model features, such as including specific bone resorption mechanisms related to the process of bone modelling and potentially distinguishing different populations of osteoblast precursors, are necessary for rat models. Furthermore, it should be emphasised that the model proposed in this paper takes into account the effects that PTH(1-34) has been suggested to have on cell numbers. However, it can certainly not be ruled out that PTH(1-34) also affects cell activities, which would imply that bone formation and resorption rates are not constant, but also dynamically depend on the availability of PTH(1-34). Such effects are, for the time being, not considered in the model, which may be an explanation for the above-mentioned inconsistencies between model predictions and experimental data. On the other hand, the current model features are believed to be sufficient to simulate PTH(1-34) treatment of osteoporosis in humans, given that bone loss and bone gain rates are far smaller in humans compared to the ones observed in small animal models (Leder et al., 2014; Tsai et al., 2015).

Finally, some remarks are made concerning computational and mathematical modelling aspects. Standardly, (not all, but many) previous modelling approaches involved the assumption that receptor-ligand binding processes are at steady state at all times, see, e.g., (Pivonka et al., 2008; 2010) and follow-up publications. In those studies, this assumption was well justified, due to the fact that receptor-ligand binding occurs much faster than the subsequent cellular responses. However, the situation is quite different when dealing with intermittent administration of PTH, as in this case the response of bone tissue (in terms of bone cell activities, and hence bone composition changes) hinges on the immediate cellular responses to an increased PTH level. Hence, in the study presented in this paper, a set of six additional ODEs had to be considered, in order to take into account the development over time of the regulatory factors of bone remodelling and modelling, see Eqs. (13) to (18). Moreover, the formulation for the expression of RANKL on osteoblast precursor cells presented in this paper is biologically more reasonable than in the aforementioned previous works, as it takes into account competitive binding effects — binding processes between RANKL RANK compete with those between RANKL and OPG — and, in addition, degradation of the complexes. Notably, the model parameters were calibrated such that for benchmark simulations, the predictions of the present model agree with the predictions of the model presented in (Pivonka et al., 2008; 2010).

5. Conclusions and outlook

The aim of the study presented in this paper was to accurately predict the development of bone tissue upon administration of PTH(1-34). For that purpose, a mathematical model was developed taking into account the dual action of PTH(1-34), differing fundamentally between intermittent and continuous administration of this drug. Considering the substantial variations in the corresponding experimental data, the model can be considered as successfully validated, see Sections 3 and 4 for presentation and discussion of the results. Hence, we deem that the pursued modelling strategy is indeed reasonable. This concerns, on the one hand, the one-compartment PK model, based on which the availability of the administered PTH(1-34) in the blood serum is estimated. As for the PD model, it seems adequate and necessary to link PTH in general, and PTH(1-34) in particular, to three mechanisms affecting the development of the bone cell populations: (i) the apoptosis of active osteoblasts, (ii) the differentiation of lining cells into active osteoblasts, and (iii) the proliferation of osteoblast precursors. In other words, considering item (ii), the results of this paper corroborate that, at least when studying rat models, it is key to take into account the influence of bone modelling (instead of restricting the model to bone remodelling effects).

Translating the mechanistic PK/PD model presented in this paper to humans is a desirable future research direction. This may render a few conceptual modifications necessary, including the reduction of the bone modelling effect. It is known that bone modelling is much more significant in small animals, such as rats, than it is in humans. Moreover, given the longer time frame of drug treatment regimes in humans, the effect of mechanical loading on bone should be probably taken into account as well. This would require additional introduction of mechanically driven regulation of the bone modelling- and remodelling-related processes which are known to be affected by their mechanical environment, see, e.g. (Scheiner et al., 2013; Lerebours et al., 2016; Pastrama et al., 2018).

Acknowledgement

Miss Silvia Trichilo acknowledges the support by The University of Melbourne, in the framework of the International PhD Scholarship Program.

Appendix A. Abbreviations

APC	adenomatous polyposis coli
Bcl-2	B-cell lymphoma 2
BCPM	bone cell population model
BV	bone volume
CREB	cAMP response element-binding protein
Dvl	dishevelled
GSK	glycogen synthase kinase 3
ODE	ordinary differential equation
OPG	osteoprotegerin
pCREB	phosphorylation of CREB
OVX	ovariectomized
PD	pharmacodynamics
PK	pharmacokinetics
PMO	postmenopausal osteoporosis
PTH	parathyroid hormone
PTH(1-34)	teriparatide
RANK	receptor of nuclear factor κB
RANKL	RANK ligand
Runx2	Runt-related transcription factor 2
TGF-β	transforming growth factor β
TV	total volume
Wnt	wingless gene

Appendix B. Analytical solutions of pharmacokinetics model

For solving Eq. (1), the administered dose is taken into account through a corresponding initial condition, $m_{\mathrm{PTH,sub}}(t_0) = d_{\mathrm{PTH}}$. Thereby, d_{PTH} is the intermittently applied dose, and it is assumed that the dose is present in the subcutaneous tissue instantaneously. Then, the solution of Eq. (1) read as

$$m_{\mathrm{PTH,sub}}(t) = d_{\mathrm{PTH}} e^{-Fk_a t}\,. \tag{25}$$

Considering Eq. (25), the solution of Eq. (2) follows as

$$C_{\mathrm{PTH,ser}}(t) = \left\{e^{-k_e t}\left[C_{\mathrm{PTH,ser}}(t_0) M_{\mathrm{PTH}} V_d (k_e - Fk_a) + d_{\mathrm{PTH}} Fk_a \left(e^{t(k_e - Fk_a)} - 1\right)\right]\right\} \times \left[M_{\mathrm{PTH}} V_d (k_e - Fk_a)\right]^{-1}. \tag{26}$$

Finally, the *AUC* follows from solution of Eq. (3), while considering both Eqs. (25) and (26), reading as

$$AUC = \left\{e^{-k_e t_{\mathrm{back}}}\left[C_{\mathrm{PTH,ser}}(t_0) M_{\mathrm{PTH}} V_d \left(e^{k_e t_{\mathrm{back}}} - 1\right) \times (k_e - Fk_a) - d_{\mathrm{PTH}}\left(Fk_a\left(e^{k_e t_{\mathrm{back}}} - 1\right) + k_e\left(e^{t_{\mathrm{back}}(k_e - Fk_a)} - e^{k_e t_{\mathrm{back}}}\right)\right)\right]\right\} \times \left[M_{\mathrm{PTH}} k_e V_d (k_e - Fk_a)\right]^{-1}, \tag{27}$$

where t_{back} is the point in time when the concentration of PTH has decayed to the background concentration, hence when $C_{\mathrm{PTH,ser}}(t) = C_{\mathrm{PTH,ser}}(t_0)$.

Appendix C. Parameters governing the coupled PK/PD model

This section is devoted to presenting all parameter values required to evaluate the mathematical framework presented in Section 2 of this paper. Calibration of the PK model has been dealt with in Section 2.1, where all involved model parameters can be found as well, see Table 2 for an overview. The parameters of the BCPM were determined based on previous model formulations (Pivonka et al., 2008; 2010), on comparing model predictions with experimental data, and based on plausibility considerations, see Tables 3–8.

Table 2
Parameters governing the PK model.

Parameter	Value	Unit
M_{PTH}	4117.8	g/mol
F	0.95	–
V_d	3.52	l
k_a	2.73	1/h
k_e	0.7	1/h

Table 3
Baseline values defining the initial conditions of the BCPM.

Parameter	Value	Unit
$C_{\mathrm{TGF\text{-}\beta}}(t_0)$	2.7×10^{-4}	pM
$C_{\mathrm{OPG}}(t_0)$	3.3×10^{-4}	pM
$C_{\mathrm{RK}}(t_0)$	9.6067	pM
$C_{\mathrm{RKL}}(t_0)$	1.2002	pM
$C_{\mathrm{PTH}}(t_0)$	10	pM
$C_{\mathrm{RK\text{-}RKL}}(t_0)$	0.3933	pM
$C_{\mathrm{OPG\text{-}RKL}}(t_0)$	40.1530	pM
$f_{\mathrm{bm}}(t_0)$	25.17	%
$C_{\mathrm{OBP}}(t_0)$	0.0035	pM
$C_{\mathrm{OBA/r}}(t_0)$	0.0011	pM
$C_{\mathrm{OBA/m}}(t_0)$	0	pM
$C_{\mathrm{OCA}}(t_0)$	7.7×10^{-5}	pM
$C_{\mathrm{OBU}}(t_0) = C_{\mathrm{OBU}}(t) = \mathrm{const.}$	10^{-3}	pM
$C_{\mathrm{OCP}}(t_0) = C_{\mathrm{OCP}}(t) = \mathrm{const.}$	10^{-3}	pM
$C_{\mathrm{LC}}(t_0) = C_{\mathrm{LC}}(t) = \mathrm{const.}$	0.0443	pM
$\tilde{c}_A(t_0)$	10	–
$\tilde{c}_B(t_0)$	10	–
$\tilde{c}_G(t_0)$	100	–

Table 4
Dissociation equilibrium constants, as well as dissociation and association rate constants included in the BCPM.

Parameter	Value	Unit
$K^{\mathrm{act}}_{\mathrm{TGF\text{-}\beta}}$	5.63×10^{-4}	pM
$K^{\mathrm{rep}}_{\mathrm{TGF\text{-}\beta}}$	1.75×10^{-4}	pM
$K^{\mathrm{act}}_{\mathrm{PTH}}$	4	pM
$K^{\mathrm{rep}}_{\mathrm{PTH}}$	0.7423	pM
$K^{\mathrm{act}}_{\mathrm{RKL}}$	16.650	pM
$k^{\mathrm{r}}_{\mathrm{OPG\text{-}RKL}}$	0.4167	1/h
$k^{\mathrm{f}}_{\mathrm{OPG\text{-}RKL}}$	8.33×10^{-4}	$(\mathrm{pM\,h})^{-1}$
$k^{\mathrm{r}}_{\mathrm{RK\text{-}RKL}}$	7.08×10^{-4}	1/h
$k^{\mathrm{f}}_{\mathrm{RK\text{-}RKL}}$	0.0030	$(\mathrm{pM\,h})^{-1}$

Table 5
Constant production and degradation rates, as well as dosage terms included in the BCPM.

Parameter	Value	Unit
β_A	6.9300	1/h
β_B	0.0999	1/h
β_G	0.6930	1/h
β_{OPG}	6.8×10^6	1/h
β_{RKL}	7000	1/h
β_{PTH}	83.160	pM/h
D_A	1	1/h
D_B	0.0096	1/h
D_G	0.6930	1/h
$D_{\mathrm{TGF\text{-}\beta}}$	0.0833	pM/h
D_{PTH}	8.3160	1/h
D_{OPG}	0.0146	1/h
D_{RKL}	0.4167	1/h
D_{RK}	0.0875	1/h
$D_{\mathrm{OPG\text{-}RKL}}$	0.4167	1/h
$D_{\mathrm{RK\text{-}RKL}}$	0.0875	1/h
$P^{\mathrm{pd}}_{\mathrm{RANKL}} = P^{\mathrm{OVX}}_{\mathrm{RANKL}}$	416.7	pM/h
$P^{\mathrm{pd}}_{\mathrm{OPG}}$	0	pM/h
$P^{\mathrm{pd}}_{\mathrm{TGF\text{-}\beta}}$	0	pM/h

Table 6
Maximum or minimum differentiation, apoptosis, and proliferation rates included in the BCPM.

Parameter	Value	Unit
$\mathcal{D}_{LC}$	0.0069	1/h
$\mathcal{D}_{OBU}$	0.0233	1/h
$\mathcal{D}_{OBP}$	0.0069	1/h
$\mathcal{D}_{OCP}$	0.0875	1/h
$\mathcal{P}_{OBP}$	0.0011	1/h
$\mathcal{A}_{OCA}$	0.2354	1/h
$\mathcal{A}_{OBA}$	0.0088	1/h

Table 7
Parameters governing the positive and negative sigmoid E_{max} functions included in the BCPM.

Parameter	Value	Unit
γ_A	1	–
α_A	2.5625	–
ρ_A	0.1250	–
δ_A	32.913	pM
γ_B	1	–
α_B	15.588	–
ρ_B	0.5	–
δ_B	317.32	pM
$\gamma_{\mathcal{A}_{OBA}}$	5	–
$\alpha_{\mathcal{A}_{OBA}}$	1.1	–
$\rho_{\mathcal{A}_{OBA}}$	0.1	–
$\delta_{\mathcal{A}_{OBA}}$	155.20	–
$\gamma_{\mathcal{P}_{OBP}}$	7	–
$\alpha_{\mathcal{P}_{OBP}}$	10	–
$\rho_{\mathcal{P}_{OBP}}$	0.9	–
$\delta_{\mathcal{P}_{OBP}}$	190.20	–
$\gamma_{\mathcal{D}_{LC}}$	30	–
$\alpha_{\mathcal{D}_{LC}}$	0.3	–
$\rho_{\mathcal{D}_{LC}}$	0	–
$\delta_{\mathcal{D}_{LC}}$	121	–

Table 8
Further parameters included in the BCPM.

Parameter	Value	Unit
α	0.01	pM
$N^{max}_{RANKL/OBP}$	2.7×10^6	–
$N_{RANK/OCP}$	10^4	–
C^{sat}_{OPG}	2×10^8	pM
$\mathcal{K}_{res}$	29.17	$(pM\,h)^{-1}$
$\mathcal{K}_{form}$	2.0419	$(pM\,h)^{-1}$

References

Bellido, T., Ali, A., Plotkin, L., Fu, Q., Gubrij, I., Roberson, P., Weinstein, R., O'Brien, C., Manolagas, S., Jilka, R., 2003. Proteasomal degradation of Runx2 shortens parathyroid hormone-induced anti-apoptotic signaling in osteoblasts — a putative explanation for why intermittent administration is needed for bone anabolism. J. Biol. Chem. 278 (50), 50259–50272.

Bringhurst, F., Demay, M., Kronenberg, H., 2016. Hormones and disorders of mineral metabolism. In: Melmed, S., Polonsky, K., Larsen, P., Kronenberg, H. (Eds.), Williams Textbook of Endocrinology. Elsevier Inc., pp. 1254–1322. Chapter 28

Buenzli, P., Pivonka, P., Gardiner, B., Smith, D., 2012. Modelling the anabolic response of bone using a cell population model. J. Theor. Biol. 307, 42–52.

Cadigan, K., Liu, Y., 2006. Wnt signaling: complexity at the surface. J. Cell Sci. 119, 395–402.

Canalis, E., Giustina, A., Bilezikian, J., 2007. Mechanisms of anabolic therapies for osteoporosis. N. Engl. J. Med. 357, 905–916.

Costa, A., Bilezikian, J., 2012. Sclerostin: therapeutic horizons based upon its actions. Curr. Osteoporos. Rep. 10, 64–72.

Danhof, M., de Jongh, J., De Lange, E., Della Pasqua, O., Ploeger, B., Voskuyl, R., 2007. Mechanism-based pharmacokinetic-pharmacodynamic modeling: biophase distribution, receptor theory, and dynamical systems analysis. Annu. Rev. Pharmacol. Toxicol. 47, 357–400.

Dempster, D., Cosman, F., Parisien, M., Shen, V., Lindsay, R., 1993. Anabolic actions of parathyroid hormone on bone. Endocr. Rev. 14, 247–250.

Dobnig, H., Turner, R., 1995. Evidence that intermittent treatment with parathyroid hormone increases bone formation in adult rats by activation of bone lining cells. Endocrinology 136, 3632–3638.

Eli Lilly & Co, 2014. FORTEO teriparatide (rbe) injection.

European Medicines Agency, 2019. Forsteo – Product Information. https://www.ema.europa.eu/en/medicines/human/epar/forsteo, last checked: March 6, 2019.

Fletcher, P., Clément, F., Vidal, A., Tabak, J., Bertram, R., 2014. Interpreting frequency responses to dose-conserved pulsatile input signals in simple cell signaling motifs. PLoS ONE 9, e95613.

Fuerer, C., Nusse, R., ten Berge, D., 2008. Wnt signalling in development and disease. EMBO Rep. 9, 134–138.

Glass, D., Bialek, P., Ahn, J., Starbuck, M., Patel, M., Clevers, H., Taketo, M., Long, F., McMahon, A., Lang, R., Karsenty, G., 2005. Canonical Wnt signaling in differentiated osteoblasts controls osteoclast differentiation. Dev. Cell 8, 751–764.

Hofbauer, L., Kühne, C., Viereck, V., 2004. The OPG/RANKL/RANK system in metabolic bone diseases. J. Musculoskelet. Neuronal Interact. 4, 268–275.

Hofbauer, L.C., Schoppet, M., 2004. Clinical implications of the osteoprotegerin/RANKL/RANK system for bone. J. Am. Med. Assoc. 292 (4), 490–495.

Huang, J., Sakata, T., Pfleger, L., Bencsik, M., Halloran, B., Bikle, D., Nissenson, R., 2004. PTH differentially regulates expression of RANKL and OPG. J. Bone Miner. Res. 19, 235–244.

Jilka, R., 2007. Molecular and cellular mechanisms of the anabolic effect of intermittent PTH. Bone 40, 1434–1446.

Kim, S., Pajevic, P., Selig, M., Barry, K., Yang, J., Shin, C., Baek, W., Kim, J., Kronenberg, H., 2012. Intermittent parathyroid hormone administration converts quiescent lining cells to active osteoblasts. J. Bone Miner. Res. 27, 2075–2084.

Komarova, S., 2005. Mathematical model of paracrine interactions between osteoclasts and osteoblasts predicts anabolic action of parathyroid hormone on bone. Endocrinology 146, 3589–3595.

Kramer, I., Halleux, C., Keller, H., Pegurri, M., Gooi, J., Weber, P., Feng, J., Bonewald, L., Kneissel, M., 2010. Osteocyte Wnt/β-catenin signaling is required for normal bone homeostasis. Mol. Cell. Biol. 30, 3071–3085.

Lauffenburger, D., Linderman, J., 1993. Receptors: Models for Binding, Trafficking,and Signaling. Oxford University Press.

Leaffer, D., Sweeney, M., Kellerman, L., Avnur, Z., Krstenansky, J., Vickery, B., Caulfield, J., 1995. Modulation of osteogenic cell ultrastructure by RS-23581, an analog of human parathyroid hormone (PTH)-related peptide-(1-34), and bovine PTH-(1-34). Endocrinology 136, 3624–3631.

Leder, B., Tsai, J., Uihlein, A., Burnett-Bowie, S.A., Zhu, Y., Foley, K., Lee, H., Neer, R., 2014. Two years of denosumab and teriparatide administration in postmenopausal women with osteoporosis (the DATA extension study): a randomized controlled trial. J. Clin. Endocrinol. Metab. 99, 1694–1700.

Lee, S.K., Lorenzo, J., 1999. Parathyroid hormone stimulates TRANCE and inhibits osteoprotegerin messenger ribonucleic acid expression in murine bone marrow cultures: correlation with osteoclast-like cell formation. Endocrinology 140, 3552–3561.

Lemaire, V., Tobin, F., Greller, L., Cho, C., Suva, L., 2004. Modeling the interactions between osteoblast and osteoclast activities in bone remodeling. J. Theor. Biol. 229, 293–309.

Lerebours, C., Buenzli, P., Scheiner, S., Pivonka, P., 2016. A multiscale mechanobiological model of bone remodelling predicts site-specific bone loss in the femur during osteoporosis and mechanical disuse. Biomech. Model. Mechanobiol. 15, 43–67.

Li, X., Liu, H., Qin, L., Tamasi, J., Bergenstock, M., Shapses, S., Feyen, J., Notterman, D., Partridge, N., 2007. Determination of dual effects of parathyroid hormone on skeletal gene expression in vivo by microarray and network analysis. J. Biol. Chem. 282, 33086–33097.

Liu, C.C., Kalu, D., 1990. Human parathyroid hormone-(1-34) prevents bone loss and augments bone formation in sexually mature ovariectomized rats. J. Bone Miner. Res. 5, 973–982.

McSheehy, P., Chambers, T., 1986. Osteoblastic cells mediate osteoclastic responsiveness to parathyroid hormone. Endocrinology 118, 824–828.

Mundy, G., Guise, T., 1999. Hormonal control of calcium homeostasis. Clin. Chem. 45, 1347–1352.

Ogura, K., Iimura, T., Makino, Y., Sugie-Oya, A., Takakura, A., Takao-Kawabata, R., Ishizuya, T., Moriyama, K., Yamaguchi, A., 2016. Short-term intermittent administration of parathyroid hormone facilitates osteogenesis by different mechanisms in cancellous and cortical bone. Bone Rep. 5, 7–14.

Pastrama, M.I., Scheiner, S., Pivonka, P., Hellmich, C., 2018. A mathematical multiscale model of bone remodeling, accounting for pore space-specific mechanosensation. Bone 107, 208–221.

Peterson, M., Riggs, M., 2010. A physiologically based mathematical model of integrated calcium homeostasis and bone remodeling. Bone 46, 49–63.

Pivonka, P., Buenzli, P., Scheiner, S., Hellmich, C., Dunstan, C., 2013. The influence of bone surface availability in bone remodelling – a mathematical model including coupled geometrical and biomechanical regulations of bone cells. Eng. Struct. 47, 134–147.

Pivonka, P., Buenzli, P.R., Dunstan, C.R., 2012. A systems approach to understanding bone cell interactions in health and disease. In: Gowder, S. (Ed.), Cell Interact., chapter 7. InTech, pp. 169–204.

Pivonka, P., Zimak, J., Smith, D., Gardiner, B., Dunstan, C., Sims, N., Martin, T., Mundy, G., 2008. Model structure and control of bone remodeling: a theoretical study. Bone 43, 249–263.

Pivonka, P., Zimak, J., Smith, D.W., Gardiner, B.S., Dunstan, C.R., Sims, N.A., Martin, T.J., Mundy, G.R., 2010. Theoretical investigation of the role of the RANK-RANKL-OPG system in bone remodeling. J. Theor. Biol. 262, 306–316.
Poole, K., van Bezooijen, R., Loveridge, N., Hamersma, H., Papapoulos, S., Löwik, C., Reeve, J., 2005. Sclerostin is a delayed secreted product of osteocytes that inhibits bone formation. FASEB J. 19, 1842–1844.
Poole, K., Reeve, J., 2005. Parathyroid hormone — a bone anabolic and catabolic agent. Curr. Opin. Pharmacol. 5, 612–617.
Potter, L., Greller, L., Cho, C., Nuttall, M., Stroup, G., Suva, L., Tobin, F., 2005. Response to continuous and pulsatile PTH dosing: a mathematical model for parathyroid hormone receptor kinetics. Bone 37, 159–169.
Potts, J., 2005. Parathyroid hormone: past and present. J. Endocrinol. 187, 311–325.
Qin, L., Raggatt, L., Partridge, N., 2004. Parathyroid hormone: a double-edged sword for bone metabolism. Trends Endocrinol. Metab. 15, 60–65.
Rattanakul, C., Lenbury, Y., Krishnamara, N., Wollkind, D., 2003. Modeling of bone formation and resorption mediated by parathyroid hormone: response to estrogen/PTH therapy. BioSystems 70, 55–72.
Satterwhite, J., Heathman, M., Miller, P., Marín, F., Glass, E., Dobnig, H., 2010. Pharmacokinetics of teriparatide (rhPTH[1-34]) and calcium pharmacodynamics in postmenopausal women with osteoporosis. Calcif. Tissue Int. 87, 485–492.
Scheiner, S., Pivonka, P., Hellmich, C., 2013. Coupling systems biology with multiscale mechanics, for computer simulations of bone remodeling. Comput. Methods Appl. Mech. Eng. 254, 181–196.
Schnoke, M., Midura, S., Midura, R., 2009. Parathyroid hormone suppresses osteoblast apoptosis by augmenting DNA repair. Bone 45, 590–602.
Sharma, S., Mahalingam, C., Das, V., Jamal, S., Levi, E., Rishi, A., Datta, N., 2013. Cell cycle and apoptosis regulatory protein (CARP)-1 is expressed in osteoblasts and regulated by PTH. Biochem. Biophys. Res. Commun. 436, 607–612.
Silva, B., Bilezikian, J., 2015. Parathyroid hormone: anabolic and catabolic actions on the skeleton. Curr. Opin. Pharmacol. 22, 41–50.
Stratford, R., Vu, C., Sakon, J., Katikaneni, R., Gensure, R., Ponnapakkam, T., 2014. Pharmacokinetics in rats of a long-acting human parathyroid hormone-collagen binding domain peptide construct. J. Pharm. Sci. 103, 768–775.
Trichilo, S., Pivonka, P., 2018. Application of disease system analysis to osteoporosis: From temporal to spatio-temporal assessment of disease progression and intervention. In: Pivonka, P. (Ed.), Multiscale Mechanobiology of Bone Remodeling and Adaptation, volume 578 of CISM International Centre for Mechanical Sciences, chapter 2. Springer, Cham., pp. 61–121.
Tsai, J., Uihlein, A., Burnett-Bowie, S.A.M., Neer, R., Zhu, Y., Derrico, N., Lee, H., Bouxsin, M., Leder, B., 2015. Comparative effects of teriparatide, denosumab, and combination therapy on peripheral compartmental bone density, microarchitecture, and estimated strength: the DATA HR-pQCT study. J. Bone Miner. Res. 30, 24–29.
U.S. Food and Drug Administration, 2019. Approved Drug Products with Therapeutic Equivalence Evaluations. 39th ed.
Wronski, T., Cintron, M., Dann, L., 1988. Temporal relationship between bone loss and increased bone turnover in ovariectomized rats. Calcif. Tissue Int. 43, 179–183.
Wronski, T., Dann, L., 1993. Parathyroid hormone is more effective than estrogen or bisphosphonates for restoration of lost bone mass in ovariectomized rats. Endocrinology 132, 823–831.
Xiong, J., O'Brien, C., 2012. Osteocyte RANKL: new insights into the control of bone remodeling. J. Bone Miner. Res. 27, 499–505.